# A non-intrusive reduced basis approach for parametrized heat transfer problems

Rachida Chakir, Yvon Maday, Philippe Parnaudeau

# A non-intrusive reduced basis approach for parametrized heat transfer problems

R. Chakir[1] , Y. Maday [2,3,4] and P. Parnaudeau[2,3]
*mail*: rachida.chakir@ifsttar.fr; maday@ljll.math.upmc.fr; philippe.parnaudeau@univ-poitiers.fr

**Abstract**

Computation Fluid Dynamics (CFD) simulation has become a routine design tool for i) predicting accurately the thermal performances of electronics set ups and devices such as cooling system and ii) optimizing configurations. Although CFD simulations using discretization methods such as finite volume or finite element can be performed at different scales, from component/board levels to larger system, these classical discretization techniques can prove to be too costly and time consuming, especially in the case of optimization purposes where similar systems, with different design parameters have to be solved sequentially. The design parameters can be of geometric nature or related to the boundary conditions. This motivates our interest on model reduction and particularly on reduced basis methods. As is well documented in the literature, the offline/online implementation of the standard RB method (a Galerkin approach within the reduced basis space) requires to modify the original CFD calculation code, which for a commercial one may be problematic even impossible. For this reason, we have proposed in a previous paper, with an application to a simple scalar convection diffusion problem, an alternative non-intrusive reduced basis approach (NIRB) based on a two-grid finite element discretization. Here also the process is two stages: *offline*, the construction of the reduced basis is performed on a fine mesh; *online* a new configuration is simulated using a coarse mesh. While such a coarse solution, can be computed quickly enough to be used in a rapid decision process, it is generally not accurate enough for practical use. In order to retrieve accuracy, we first project every such coarse solution into the reduced space, and then further improve them via a rectification technique. The purpose of this paper is to generalize the approach to a CFD configuration.

**Keywords** : Non-intrusive method; Reduced basis method; Parametric studies; Heat transfer; CFD.

## 1. Introduction

During the past fifty years electronic devices and systems kept becoming smaller and smaller, this growing need for miniaturization led to an increasing high heat production. To avoid any possible failure or malfunction of electronics devices and ensure their reliability, it is essential to maintain the temperature of the electronic components below an acceptable upper limit. Cooling of electronic systems is consequently essential in controlling the component temperature and avoiding any hot spot. Designing cooling systems for miniaturized electronics devices presents difficult challenges to mechanical engineers and analysts. Average while, computational modeling is gaining popularity, particularly Computation

[1]Université Paris Est, IFSTTAR, 10-14 Bd Newton, Cité Descartes, 77447 Marne La Vallée Cedex, France
[2]CNRS, UMR 7598, Laboratoire Jacques-Louis Lions, F-75005, Paris, France
[3]UPMC Univ Paris 06, UMR 7598, Laboratoire Jacques-Louis Lions, F-75005, Paris, France
[4]Institut Universitaire de France and Division of Applied Mathematics, Brown University, Providence, RI, USA

Fluid Dynamics (CFD) modeling which has become a routine design tool for predicting accurately thermal performance of electronics cooling system. Although CFD modeling can be used at different scales, from component/board levels to larger system, classical discretization techniques such as finite volume or finite element methods can prove to be limited by memory space and long calculation times, which can be problematic. Inexpensive and accurate computational tools to predict the fluid flow and heat transfer can be very useful, specially when thermal analysis is done at the end of the design process where time constraints are greatest, hence our focus on model reduction and particularly to reduced basis methods (see [9, 14, 17, 19]).

Reduced basis method exploits the parametric structure of the governing PDEs to construct rapidly, convergent and computationally efficient approximations. Previous work on the reduced basis method in numerical fluid dynamics has been carried out by [12, 16, 20] and more particularly for the Navier-Stokes equations [7, 18, 23, 27, 28] which requires treatment of non-linearity and non-affine parametric dependence. More recent works with turbulent flows can be found in [2, 26]. Let $\sigma$ be a set of parameters associated to our physical system, these methods rely on the fact that when the parameters vary, the manifold of solutions is often of small (Kolmogorov) dimension. In this instance, there exists a set of $N$ particular values of $\sigma$ taken in $\mathcal{D}$ (the parameter space) from which one can build a basis. This basis, called reduced basis, is made of the solutions $u(\sigma_1), \cdots, u(\sigma_N)$ and can approach any solution $u(\sigma)$, $\sigma \in \mathcal{D}$. Thus, when the $\sigma_i$ are well chosen[5], the size of the reduced basis is much smaller compared to the number of degrees of freedom of the problem discretized by a classical method (finite element, finite volume, or other). The standard reduced basis method is a Galerkin approach within the reduced basis approximation space, thus the reduced basis approximation of the "truth" solution is obtained by the resolution of a small dimensional linear system. One of the keys of this technique is the decomposition of the computational work into *offline/online* stages. However, the decomposition of the matrices into *offline/online* pieces requires modifying the calculation code, leading to an intrusive procedure. Examples of the standard reduced basis method applied to heat transfer problems can be found in [8, 21, 24, 25]. In some situation — with a commercial CFD code for example – it is not possible to perform all the *offline* computations required to have a inexpensive and fast *online* stage. For this reason, we proposed to use an less intrusive reduced basis method, introduced in [3, 4], where coarse triangulations are used to compute coarse approximation during the *online* stage. Recently, other non-intrusive Reduced Order Methods (ROM) for fluid dynamics have been proposed [5, 29], those ROM are based on proper orthogonal decomposition and Radial Basis function (RBF) to compute the coefficients of the reduced model. During the online computation, for any given (untrained) parameter an interpolation approach using RBF as interpolation functions is used to estimate the coefficients of the POD decomposition. As in our method we use coarse triangulations to compute coefficients of the RB decomposition and then further improve them via a rectification technique, keeping a physical meaning to the approach.

The aim of this paper is to provide tests to validate and generalize our method for heat transfer problems. In Section 2, we provide a brief introduction to reduced basis methods and the methodology of the non-intrusive reduced basis method. In Section 3, we give a brief description of simple models of cooling devices; we formulate the physical system, the governing equations and boundary conditions. In Section 4, we discuss our numerical experimentations and present the results and conclusions.

[5] A classical and efficient approach to choose the $\sigma_i$ is the greedy method [1, 11].

## 2. Methodology

Let us consider the nonlinear parametrized PDEs describing our physical system, over a bounded domain $\Omega \subset \mathbb{R}^d$, $d = 2$ or 3. In these governing equations, $\theta$ represent the temperature, $u_i$ the components of the velocity vector field $\mathbf{u}$ in the $x_i$-directions , $p$ the pressure and $\sigma$ is a set of $n_p$ parameters related to physical properties or boundary conditions. We denote by $\mathcal{D} \subset \mathbb{R}^{n_p}$ the set of parameters.
We now introduce the variational formulation of our parametrized PDEs :

$$\begin{cases} \text{for a given } \sigma \in \mathcal{D}, \text{ find } (\theta, \mathbf{u}, p) \equiv (\theta(\sigma), \mathbf{u}(\sigma), p(\sigma)) \in X \times Y \times Q \text{ such that} \\ \mathcal{F}(\theta, \mathbf{u}, p\,; T, \mathbf{v}, q;\, \sigma) = (0, \mathbf{0}, 0)^t, \qquad \forall\, (T, \mathbf{v}, q) \in X \times Y \times Q, \end{cases} \tag{1}$$

where $\mathcal{F}$ is a functional with the appropriate properties, $X, Y$ and $Q$ are appropriate functional spaces. Let $\{\mathcal{T}_h\}_h$ be a family of regular triangulation of $\Omega$, we denote by $X_h$, $Y_h$ and $Q_h$ finite element approximation subspaces of respectively $X$, $Y$ and $Q$ over $\mathcal{T}_h$. The discrete velocity space $Y_h$ and the discrete pressure space $Q_h$ are chosen in order to satisfy the inf-sup condition [6, 13, 22].
The finite element discretization of (1) is as follows :

$$\begin{cases} \text{for a given } \sigma \in \mathcal{D}, \text{ find } (\theta_h, \mathbf{u}_h, p_h) \equiv (\theta_h(\sigma), \mathbf{u}_h(\sigma), p_h(\sigma)) \in X_h \times Y_h \times Q_h \text{ such that} \\ \mathcal{F}(\theta_h, \mathbf{u}_h, p_h\,; T, \mathbf{v}, q;\, \sigma) = (0, \mathbf{0}, 0)^t, \qquad \forall\, (T, \mathbf{v}, q) \in X_h \times Y_h \times Q_h, \end{cases} \tag{2}$$

For significantly fine meshes $\mathcal{T}_h$ and adequately chosen discretization spaces $X_h$, $Y_h$ and $Q_h$, the conforming finite element solution $(\theta_h, \mathbf{u}_h, p_h)$, solution to (2), is accurate enough to be considered as a good approximation of the exact solution, named "truth solutions". However, because of the high dimension of the associated discretization spaces, solving the finite element problem (2) with different values of $\sigma$ can prove to be too costly and time consuming.
The idea of reduced basis methods is to provide an economical and accurate approximation to the "truth" approximation $(\theta_h, \mathbf{u}_h, p_h)$ by using approximation spaces made up of few suitable samples of solutions to the parametrized PDEs. This relies on the fact that when the parameters vary, the set of solutions is often of small Kolmogorov width, thus implying that the manifold of all solutions can be approximated within a (small) finite space of well-chosen solutions to the parametrized problem (2). In that case, there exists a set of parameters $S_N = (\sigma_1, \sigma_2, \cdots, \sigma_N) \in \mathcal{D}^N$ such that for any $\sigma \in \mathcal{D}$, the truth solution can be approximated by a linear combination of the particular solutions associated to $\sigma_i \in S_N$.
To distinguish each physical component (temperature, velocity and pressure), we add superscripts $\theta$, $\mathbf{u}$ or $p$ in our notation, for example we denote by $(\sigma_1^\theta, \sigma_2^\theta, , \cdots, \sigma_{N^\theta}^\theta)$ the set of parameters — with size $N^\theta$ — used to generate the reduced basis approximation space associated to the temperature component of the solution. For each physical component, we introduce the associated reduced basis approximation spaces as

$$\begin{aligned} X_h^N &= \text{span}\{\theta_h(\sigma_i^\theta), 1 \le i \le N^\theta\} = \text{span}\{\phi_i^\theta,\, 1 \le i \le N^\theta\}, \\ Y_h^N &= \text{span}\{\mathbf{u}_h(\sigma_i^\mathbf{u}), 1 \le i \le N^\mathbf{u}\} = \text{span}\{\phi_i^\mathbf{u},\, 1 \le i \le N^\mathbf{u}\}, \\ Q_h^N &= \text{span}\{p_h(\sigma_i^p), 1 \le i \le N^p\} = \text{span}\{\phi_i^p,\, 1 \le i \le N^p\}, \end{aligned}$$

where the $\left(\phi_i^\theta\right)_i \in X_h$, $(\phi_i^\mathbf{u})_i \in Y_h$, $(\phi_i^p)_i \in Q_h$ are $H^1$-orthonormal basis sets (obtained respectively from $\left(\theta_h(\sigma_i^\theta)\right)_i$, $(\mathbf{u}_h(\sigma_i^\mathbf{u}))_i$ and $(p_h(\sigma_i^p))_i$ by a orthogonalization process), called reduced basis functions. The standard reduced basis method consists in a Galerkin approach within the low dimensional spaces $X_h^N$, $Y_h^N$ and $Q_h^N$.

$$\left\{\begin{array}{l} \text{for a given } \sigma \in \mathcal{D}, \text{ find } (\theta_h^N, \mathbf{u}_h^N, p_h^N) \in X_h^N \times Y_h^N \times Q_h^N \text{ such that} \\ \mathcal{F}(\theta_h^N, \mathbf{u}_h^N, p_h^N; T, \mathbf{v}, q; \sigma) = (0, \mathbf{0}, 0)^t, \qquad \forall\, (T, \mathbf{v}, q) \in X_h^N \times Y_h^N \times Q_h^N. \end{array}\right. \tag{3}$$

Note that, in order to ensure stable, good approximation of the pressure, supremizer-enrichment of the velocity reduced basis space may be performed, see for example [6, 13, 22][6].
One of the key ingredients of the method is the decomposition of the computational work into *offline* and *online* stages. During the *offline* stage the reduced basis functions are computed — providing the above defined spaces $X_h^N, Y_h^N, Q_h^N$ — as well as all parameter-independent quantities. This is an expensive stage that is done only once, whereas parameter-dependent quantities are computed during the *online* stage together with the resolution to (3). Considering that the dimension of the reduced basis space is quite smaller compared to the finite element one, solving the reduced problem (3) is much less expensive than the "truth" finite element problem (2).

The construction of the associated discrete system to be solved is thus classically the corner stone of the global process. Indeed, since the construction of the reduced discrete system associated to the variational form $\mathcal{F}(\theta_h^N, \mathbf{u}_h^N, p_h^N; T, v, q; \sigma)$ has to be done for each new value of $\sigma$, to perform efficiently the online stage, one has to be able to isolate the parametric contributions. Thus, all $\sigma$-independent quantities, high dimensional matrices and vectors used in the construction of the reduced discrete system are computed only once and saved during the offline stage. This part of the offline stage requires entering and modifying the simulation code used to compute the truth finite element approximations, leading to an intrusive method, which can be problematic. When the simulation code is locked and used as a black box — which is often the case in the industrial framework — the parametric decomposition is not possible, which prevent us from building each new reduced discrete system quickly for a new value of $\sigma$. This take away the benefit of the reduced basis method, thus to overcome it, we propose to use an alternative method, less intrusive, where coarse triangulations are used to compute finite element solutions during the *online* stage. These "coarse" approximations are projected into the reduced basis approximation spaces $X_h^N, Y_h^N, Q_h^N$, and then improve via a rectification technique introduced in [3, 4]. All these improvements after the coarse approximation is computed can be done in a different, more versatile code than the one used to do the simulation.
Let $\{\mathcal{T}_H\}_H$ be a family of "coarse" regular triangulation of $\Omega$, such that $H >> h$, we denote by $X_H$, $Y_H$ and $Q_H$ the coarse finite element spaces associated to this mesh, and $(\theta_H, \mathbf{u}_H, p_H)$ the "coarse" finite element approximation. Since the computation of the "coarse" finite element approximation, for $H >> h$ is less expensive than the "truth" approximation, using the simulation code — during the online stage — with the mesh size $H$ (chosen adequately) to construct a reduced solution is still cheap enough.

In order to understand our non-intrusive reduced basis method, let us indicate that the idea of standard reduced basis methods (3) is to compute an inexpensive and accurate approximation of the projection of the solution $(\theta_h(\sigma), \mathbf{u}_h(\sigma), p_h(\sigma))$ on $X_h^N \times Y_h^N \times Q_h^N$, by evaluating the coefficients appearing in the decomposition of $\theta_h^N(\sigma)$, $\mathbf{u}_h^N(\sigma)$ and $p_h^N(\sigma)$ in the basis $\left(\phi_i^\theta\right)_i$, $(\phi_i^{\mathbf{u}})_i$ and $(\phi_i^p)_i$.

The best linear combination – measured in $H^1$-norm – of the reduced basis functions is provided by the $H^1$-orthogonal projection
In our method, an alternative linear combination of the reduced basis functions has been chosen, using

[6]However, in our context, we are not much interested here in the precise value of the pressure that is (only) a Lagrange multiplier to the divergence free condition), thus using the fact that the reduced velocity space is composed of divergence free functions the pressure does not even appear in the reduced set of equations (3), if no supremizer for the pressure space is added to $X_h^N$.

the optimal coefficients $\{\beta_j^{\theta,h}(\sigma)\}_{1\leq j\leq N_\theta}$ and $\{\beta_j^{\mathbf{u},h}(\sigma)\}_{1\leq j\leq N_\mathbf{u}}$ involved in the $L^2$-orthogonal projection of $\theta_h(\sigma)$ on $X_h^N$ and $\mathbf{u}_h(\sigma)$ on $Y_h^N$. As shown in [3, 4], these coefficients, defined as follows

$$\beta_i^{\theta,h}(\sigma) = \left(\theta_h(\sigma), \phi_i^\theta\right)_{L^2}, \quad \text{and} \quad \beta_j^{\mathbf{u},h}(\sigma) = \left(\mathbf{u}_h(\sigma), \phi_j^\mathbf{u}\right)_{L^2} \qquad \text{with } 1\leq i\leq N^\theta \text{ and } 1\leq j\leq N^\mathbf{u}, \tag{4}$$

are still good enough but require the knowledge of the fine solution intervening respectively in the decomposition of $\theta_h(\sigma)$ and $\mathbf{u}_h(\sigma)$. The non-intrusive reduced basis method aims at computing a cheap, yet accurate enough approximation of these coefficients by using

$$\beta_i^{\theta,H}(\sigma) = \left(\theta_H(\sigma), \phi_i^\theta\right)_{L^2}, \quad \text{and} \quad \beta_j^{\mathbf{u},H}(\sigma) = \left(\mathbf{u}_H(\sigma), \phi_j^\mathbf{u}\right)_{L^2} \qquad \text{with } 1\leq i\leq N^\theta \text{ and } 1\leq j\leq N^\mathbf{u}, \tag{5}$$

as substitutes. While "coarse" finite element approximations $(\theta_H(\sigma), \mathbf{u}_H(\sigma))$ can be computed quickly enough to be used in model reduction techniques, they may not be accurate enough for practical use. We have proven in [3, 4] on a simpler example that this first NIRB approximation provides some improvement in the accuracy with respect to the coarse solution. To further improve the accuracy of this technique we have also proposed to perform a simple "rectification" that allows to ensure that, for the set of parameters $S_{N^\theta} \equiv \{\sigma_i^\theta\}_{i,\,1\leq i\leq N^\theta}$, (and resp. $S_{N^\mathbf{u}} \equiv \{\sigma_i^\mathbf{u}\}_{i,\,1\leq i\leq N^\mathbf{u}}$) used in the construction of the reduced basis, the method returns exactly $\theta_h(\sigma_i^\theta)$ (and resp. $\mathbf{u}_h(\sigma_i^\mathbf{u})$). Indeed, contrarily to $\theta_h(\sigma)$ and $\mathbf{u}_h(\sigma)$ that we don't want to compute for a large number of values of $\sigma$, the set $\{\theta_h(\sigma_i^\theta)\}_{i,\,1\leq i\leq N^\theta}$ and $\{\mathbf{u}_h(\sigma_i^{N_\mathbf{u}})\}_{i,\,1\leq i\leq N^\mathbf{u}}$ have actually already been computed to build the reduced basis spaces. It is thus desirable that the non-intrusive reduced basis approach provides these truth solutions. To do so, we need to identify the matrices $R^{\theta,N}\in\mathbb{R}^{N_\theta\times N_\theta}$ and $R^{\mathbf{u},N}\in\mathbb{R}^{N_\mathbf{u}\times N_\mathbf{u}}$ such that :

$$\sum_{j=1}^{N_\theta} R_{ij}^{\theta,N}\,\beta_j^{\theta,H}(\sigma_k^\theta) = \beta_i^{\theta,h}(\sigma_k^\theta), \qquad \forall\, 1\leq i\leq N_\theta, \quad \forall \sigma_k^\theta\in S_{N^\theta},$$

$$\sum_{j=1}^{N_\mathbf{u}} R_{ij}^{\mathbf{u},N}\,\beta_j^{\mathbf{u},H}(\sigma_k^\mathbf{u}) = \beta_i^{\mathbf{u},h}(\sigma_k^\mathbf{u}), \qquad \forall\, 1\leq i\leq N_\mathbf{u}, \quad \forall \sigma_k^\mathbf{u}\in S_{N^\mathbf{u}}.$$

So that for each new value of $\sigma$, we can replace the $\beta_i^{\theta,H}(\sigma)$ and $\beta_i^{\mathbf{u},H}(\sigma)$ coefficients by respectively

$$\beta_i^{\theta_{H,h}}(\sigma) = \sum_{j=1}^{N_\theta} R_{ij}^{\theta,N}\,\beta_j^{\theta,H}(\sigma)$$

and

$$\beta_i^{\mathbf{u}_{H,h}}(\sigma) = \sum_{j=1}^{N_\mathbf{u}} R_{ij}^{\mathbf{u},N}\,\beta_j^{\mathbf{u},H}(\sigma),$$

to eventually build an improved non-intrusive reduced basis approximation

$$\begin{cases} \theta_{H,h}^N &= \displaystyle\sum_{i,j=1}^{N_\theta} R_{ij}^{\theta,N}\beta_j^{\theta,H}(\sigma)\,\phi_i^{\theta,N} \\ \\ \mathbf{u}_{H,h}^N &= \displaystyle\sum_{i,j=1}^{N_\mathbf{u}} R_{ij}^{\mathbf{u},N}\beta_j^{\mathbf{u},H}(\sigma)\,\phi_i^{\mathbf{u},N}. \end{cases} \tag{6}$$

In our previous work, we took the matrix $R^{\theta,N}$ equal to

$$R^{\theta,N} = \left(\begin{array}{c|c|c} \beta_1^{\theta,h}(\sigma_1^\theta) & \cdots & \beta_1^{\theta,h}(\sigma_{N_\theta}^\theta) \\ \vdots & \vdots & \vdots \\ \beta_{N_\theta}^{\theta,h}(\sigma_1^\theta) & \cdots & \beta_{N_\theta}^{\theta,h}(\sigma_{N_\theta}^\theta) \end{array}\right) \times \left(\begin{array}{c|c|c} \beta_1^{\theta,H}(\sigma_1^\theta) & \cdots & \beta_1^{\theta,H}(\sigma_{N_\theta}^\theta) \\ \vdots & \vdots & \vdots \\ \beta_{N_\theta}^{\theta,H}(\sigma_1^\theta) & \cdots & \beta_{N_\theta}^{\theta,H}(\sigma_{N_\theta}^\theta) \end{array}\right)^{-1} \tag{7}$$

and the matrix $R^{\mathbf{u},N}$ is equal to

$$R^{\mathbf{u},N} = \left(\begin{array}{c|c|c} \beta_1^{\mathbf{u},h}(\sigma_1^\mathbf{u}) & \cdots & \beta_1^{\mathbf{u},h}(\sigma_{N_\mathbf{u}}^\mathbf{u}) \\ \vdots & \vdots & \vdots \\ \beta_{N_\mathbf{u}}^{\mathbf{u},h}(\sigma_1^\mathbf{u}) & \cdots & \beta_{N_\mathbf{u}}^{\mathbf{u},h}(\sigma_{N_\mathbf{u}}^\mathbf{u}) \end{array}\right) \times \left(\begin{array}{c|c|c} \beta_1^{\mathbf{u},H}(\sigma_1^\mathbf{u}) & \cdots & \beta_1^{\mathbf{u},H}(\sigma_{N_\mathbf{u}}^\mathbf{u}) \\ \vdots & \vdots & \vdots \\ \beta_{N_\mathbf{u}}^{\mathbf{u},H}(\sigma_1^\mathbf{u}) & \cdots & \beta_{N_\mathbf{u}}^{\mathbf{u},H}(\sigma_{N_\mathbf{u}}^\mathbf{u}) \end{array}\right)^{-1}. \tag{8}$$

However when $N_\theta$ is large (and resp. $N_\mathbf{u}$), we have observed that the rectification process is less robust when the matrix $R^{\theta,N}$ (and resp . $R^{\mathbf{u},N}$) is calculated according to (7) (and resp.(8)).
The challenge is to find an easy way to compute the rectification matrices while retaining good approximation. We use an approach based on a regularized least-square method. For $1 \leq i \leq N$, we introduce:
- the vectors $\mathcal{R}_i^{\theta,N} \in \mathbb{R}^{N_\theta}$ and $\mathcal{R}_i^{\mathbf{u},N} \in \mathbb{R}^{N_\mathbf{u}}$ respectively defined by

$$\{\mathcal{R}_i^{\theta,N}\}_j = R_{ij}^{\theta,N} \text{ and } \{\mathcal{R}_i^{\mathbf{u},N}\}_j = R_{ij}^{\mathbf{u},N}, \forall 1 \leq j \leq N,$$

- the vectors $\mathcal{B}_i^{\theta,N} \in \mathbb{R}^{N_\theta}$ and $\mathcal{B}_i^{\mathbf{u},N} \in \mathbb{R}^{N_\mathbf{u}}$ respectively defined by

$$(\mathcal{B}_i^{\theta,N})_k = \beta_i^{\theta,h}(\sigma_k^\theta), \qquad \forall \sigma_k^\theta \in S_{N^\theta}$$

and

$$(\mathcal{B}_i^{\mathbf{u},N})_k = \beta_i^{\mathbf{u},h}(\sigma_k^\mathbf{u}), \qquad \forall \sigma_k^\mathbf{u} \in S_{N^\mathbf{u}}.$$

- the matrices $\mathcal{H}^{\theta,N} \in \mathbb{R}^{N_\theta \times N_\theta}$ and $\mathcal{H}^{\mathbf{u},N} \in \mathbb{R}^{N_\mathbf{u} \times N_\mathbf{u}}$ respectively defined by

$$\mathcal{H}^{\theta,N} = \left(\begin{array}{c|c|c} \beta_1^{\theta,H}(\sigma_1^\theta) & \cdots & \beta_{N_\theta}^{\theta,H}(\sigma_1^\theta) \\ \vdots & \vdots & \vdots \\ \beta_1^{\theta,H}(\sigma_{N_\theta}^\theta) & \cdots & \beta_{N_\theta}^{\theta,H}(\sigma_{N_\theta}^\theta) \end{array}\right) \quad \text{and} \quad \mathcal{H}^{\mathbf{u},N} = \left(\begin{array}{c|c|c} \beta_1^{\mathbf{u},H}(\sigma_1^\mathbf{u}) & \cdots & \beta_{N_\mathbf{u}}^{\mathbf{u},H}(\sigma_1^\mathbf{u}) \\ \vdots & \vdots & \vdots \\ \beta_1^{\mathbf{u},H}(\sigma_{N_\mathbf{u}}^\mathbf{u}) & \cdots & \beta_{N_\mathbf{u}}^{\mathbf{u},H}(\sigma_{N_\mathbf{u}}^\mathbf{u}) \end{array}\right)$$

Our rectification approach consists in looking for the vectors $R_i^{\theta,N}$ and $R_i^{\mathbf{u},N}$ which respectively minimize the cost functions

$$C_i^{\theta,N} = \|\mathcal{H}^{\theta,N}\mathcal{R}_i^{\theta,N} - \mathcal{B}_i^{\theta,N}\|_2^2 + \lambda\|\mathcal{R}_i^{\theta,N}\|_2^2, \quad \text{for } 1 \leq i \leq N \tag{9}$$

and

$$C_i^{\mathbf{u},N} = \|\mathcal{H}^{\mathbf{u},N}\mathcal{R}_i^{\mathbf{u},N} - \mathcal{B}_i^{\mathbf{u},N}\|_2^2 + \lambda\|\mathcal{R}_i^{\mathbf{u},N}\|_2^2, \quad \text{for } 1 \leq i \leq N, \tag{10}$$

where $\lambda$ is a regularization term and $\|\cdot\|_2$ stand for the Euclidian $\ell_2$-norm.

## 3. Application to heat transfer and CFD problems

One of the most prominent industrial applications of heat transfer problems is the cooling and thermal control of electronic devices and circuitry. Cooling systems are generally divided into two categories: passive (rely on the thermo-dynamics of conduction and convection to complete the heat transfer process) and active (require an external powered device as fans or pumps). In these paper we choose to study the heat transfer due to natural convection in a heated cavity and heat transfer inside a simple cooling system for electronics components.

### *3.1. The governing equations*

The fluid is supposed incompressible and driven by external forces – the gravity acting on the mass. The governing equations are the stationary Navier-Stokes equations, in the Cartesian coordinates they are given by :

- Continuity equation :

$$\nabla \cdot \mathbf{u} = 0 \tag{11}$$

- Time independent momentum equation :

$$\rho\Big(\mathbf{u}\cdot\nabla\mathbf{u}\Big) - \mu\,\Delta\mathbf{u} + \nabla p = \rho\,\mathbf{g} \tag{12}$$

- Time independent thermal energy equation :

$$\rho\,C_p\Big(\mathbf{u}\cdot\nabla\theta\Big) - k\,\Delta\theta = 0 \tag{13}$$

| | | | |
|---|---|---|---|
| $\rho$ | density | $C_p$ | heat capacity |
| $k$ | thermal conductivity | $\mu$ | dynamic viscosity |
| $\kappa$ | thermal diffusivity $(= \frac{k}{\rho C_p})$ | $\nu$ | kinematic viscosity $(= \frac{\mu}{\rho})$ |

Table 1: Nomenclature of fluid's properties

Considering a reference state in which the density $\rho_{\text{ref}}$ and the pressure $p_{\text{ref}}$ are so that $\nabla p_{\text{ref}} = \rho_{\text{ref}}\,\mathbf{g}$ and writing $p = p_{\text{ref}} + \tilde{p}$ and $\rho = \rho_{\text{ref}} + \tilde{\rho}$, equation (12) becomes

$$\Big(1 + \tfrac{\tilde{\rho}}{\rho_{\text{ref}}}\Big)\Big(\mathbf{u}\cdot\nabla\mathbf{u}\Big) + \tfrac{1}{\rho_{\text{ref}}}\nabla\tilde{p} - \nu_{\text{ref}}\;\Delta\mathbf{u} = \tfrac{\tilde{\rho}}{\rho_{\text{ref}}}\;\mathbf{g}, \qquad \text{with } \nu_{\text{ref}} = \frac{\mu}{\rho_{\text{ref}}},$$

and equation (13) becomes

$$\Big(1 + \tfrac{\tilde{\rho}}{\rho_{\text{ref}}}\Big)\Big(\mathbf{u}\cdot\nabla\theta\Big) - \kappa_{\text{ref}}\;\Delta\theta = 0, \qquad \text{with } \kappa_{\text{ref}} = \frac{k}{\rho_{\text{ref}}\,C_p},$$

We place ourselves within the *Boussinesq approximation*[7] for steady state, with

$$\tilde{\rho} = \rho_{\text{ref}}\,\beta\ (\theta - \theta_{\text{ref}}),$$

where $\beta$ is the volumetric coefficient of the thermal expansion and $\theta_{\text{ref}}$ some reference temperature for which $\rho_{\text{ref}} = \rho$, here we took $\theta_{\text{ref}} = 295$ Kelvin's degrees. By applying this approximation, the momentum equation (12) becomes :

$$\mathbf{u}\cdot\nabla\mathbf{u} + \frac{1}{\rho_{\text{ref}}}\nabla\tilde{p} - \nu_{\text{ref}}\ \Delta\mathbf{u} = \beta(\theta - \theta_{\text{ref}})\,\mathbf{g}, \tag{14}$$

and the thermal energy equation (13) becomes

$$-\kappa_{\text{ref}}\,\Delta\theta + \mathbf{u}\cdot\nabla\theta = 0. \tag{15}$$

*3.2. Application 1 : Natural convection in a 2D cavity*

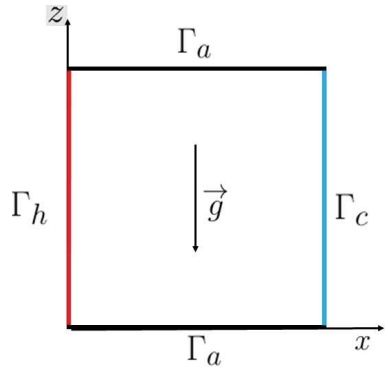


Figure 1: Geometry for a differentially heated square cavity

In this first example we investigate the case of a flow enclosed in a two-dimensional $(x, z)$ differentially heated square cavity (see Figure 1). The left wall is maintained at the hot temperature $T_h$, the right one at the cold temperature $T_c = T_{ref}$ whereas the walls at top and bottom are adiabatic.
The governing equations (11),(15) and (14) are made dimensionless by introducing $\Delta\theta = T_h - T_c$ (the temperature difference), $L$ (the distance between region of high temperature and region of low temperature), the Grashof number $Gr = \dfrac{g\beta\Delta\theta L^2}{\nu^2}$ (the ratio between the buoyant forces and viscous forces acting on the fluid) and the Prandtl number $Pr = \dfrac{\nu}{\kappa}$ (the ratio between the kinematic viscosity and the thermal diffusivity). The following dimensionless quantities are introduced:

$$X = \frac{x}{L}, \quad Z = \frac{z}{L}, \quad \mathbf{U} = \frac{\mathbf{u}}{\sqrt{g\beta\Delta\theta L}}, \quad P = \frac{\tilde{p}}{g\beta\Delta\theta L\rho_{ref}}, \quad \Theta = \frac{\theta - T_c}{T_h - T_c}$$

[7]Boussinesq approximation states that the thermo-physical properties of the fluid ($\rho$, $\mu$, $C_p$ and $k$) are assumed to be constant and independent of temperature except in the gravity term. Hence the variation of the density $\frac{\tilde{\rho}}{\rho_{\text{ref}}}$ due to changes in the temperature can be neglected except in the gravity term.

The dimensionless velocity $\mathbf{U} = (u_x, u_z)$, the dimensionless temperature $\theta$, the pressure $p$ of the fluid satisfy the following equations :

$$\begin{cases} -\dfrac{1}{\sqrt{Gr}}\Delta\mathbf{U} + \mathbf{U}\cdot\nabla\mathbf{U} + \nabla P &= (0,1)^T\,\Theta & \text{in } \Omega, \\ \nabla\cdot\mathbf{U} &= 0 & \text{in } \Omega, \\ \mathbf{U} &= 0 & \text{on } \partial\Omega, \\ \\ -\dfrac{1}{Pr\sqrt{Gr}}\,\Delta\Theta + \mathbf{U}\cdot\nabla\Theta &= 0 & \text{in } \Omega, \\ \Theta &= 0 & \text{on } \Gamma_c, \\ \Theta &= 1 & \text{on } \Gamma_h, \\ \dfrac{\partial\Theta}{\partial n} &= 0 & \text{on } \Gamma_a. \end{cases} \tag{16}$$

The varying parameters of this example are the Grashof number $Gr \in [10^3, 10^6]$ and the Prandtl number $Pr \in [0.5, 1]$.

### *3.3. Application 2 : Cooling system of electronic devices*

In this second example we are interested by the variation of the temperature in a simplified system that is inspired by a suggested cooling system for electronic device (a small box with two electronic components).

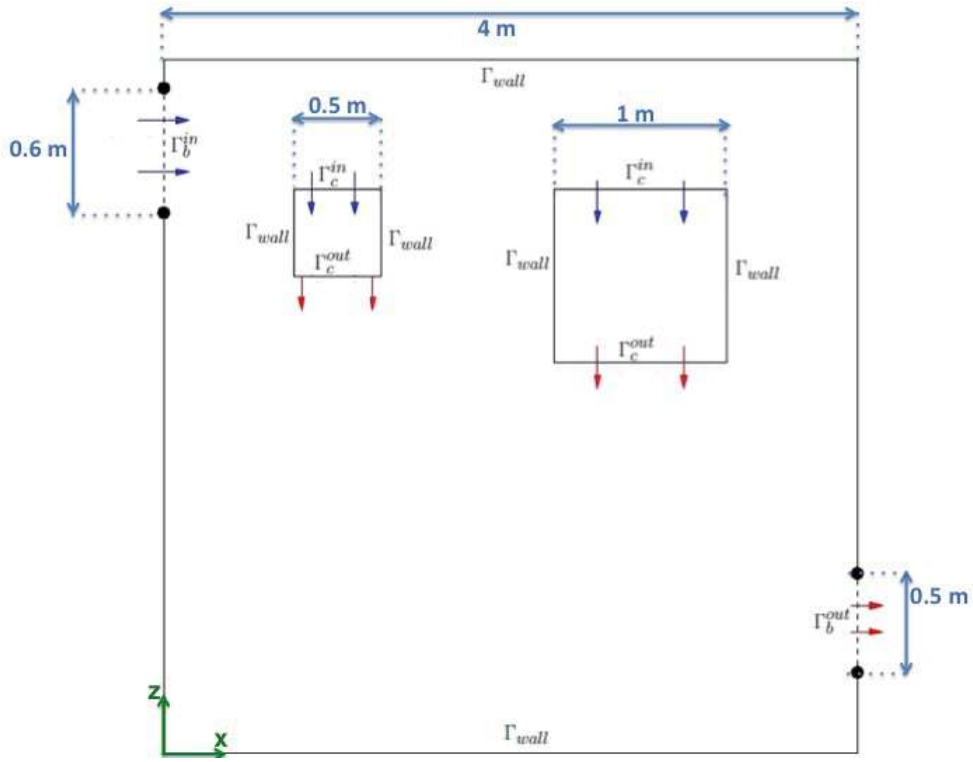


Figure 2: Geometry of the simplified cooling system for electronic devices

The model is a two dimensional square where the cooling air enters the box at the $\Gamma_b^{in}$ boundary and flows around the two electronic components. Those two components produce heat energy at the boundary $\Gamma_c^{\text{out}}$, and due to a convection phenomenon the heat energy is carried out by the fluid flow through the box to finally exits from the boundary $\Gamma_b^{out}$ (see Figure 2).

On the inflow section $\Gamma_b^{in}$ a Poiseuille's velocity profile $\mathbf{v}_{in} = v_b \begin{pmatrix} f(x) \\ 0 \end{pmatrix}$ is imposed, where $v_b$ is the velocity magnitude and $f(x)$ a parabolic function. On the outflow section $\Gamma_b^{out}$, homogenous Neumann condition is imposed. For the flow passing through the electronic components, we have chosen to model the interaction by non homogenous Dirichlet condition $v_c$ imposed to the second component of the velocity on the inflow $\Gamma_c^{in}$ and similarly on the outflow sections $\Gamma_c^{out}$.
We impose a temperature of $\theta_b$ on the inflow section $\Gamma_b^{in}$ and a temperature of $\theta_c$ on the outflow section $\Gamma_c^{out}$, whereas the walls $\Gamma_{wall}$, the outflow section $\Gamma_b^{out}$ and the inflow section $\Gamma_c^{in}$ are all adiabatic.

The velocity $\mathbf{u} = (u_x, u_z)$, the temperature $\theta$, the pressure $p$ of the fluid satisfy the following equations :

$$
\left\{
\begin{array}{rcll}
\nabla \cdot \mathbf{u} & = & 0, & \\
\mathbf{u}.\nabla \mathbf{u} + \dfrac{1}{\rho_{ref}} \nabla \tilde{p} - \nu_{\text{ref}} \, \Delta \mathbf{u} & = & \beta(\theta - \theta_{\text{ref}}) \, \mathbf{g}, & \\
\mathbf{u} \cdot \nabla \theta - \kappa_{\text{ref}} \, \Delta \theta & = & 0, & \\
 & & & \\
\mathbf{u} & = & \mathbf{v}_{in} & \text{on} \quad \Gamma_b^{in} \\
\dfrac{\partial \mathbf{u}}{\partial n} & = & 0 & \text{on} \quad \Gamma_b^{out} \\
\mathbf{u} & = & \mathbf{0} & \text{on} \quad \Gamma_{wall} \\
u_z = -v_c \,, \; u_x & = & 0 & \text{on} \quad \Gamma_c^{out} \\
u_z = -v_c \,, \; \dfrac{\partial u_x}{\partial n} & = & 0 & \text{on} \quad \Gamma_c^{in} \\
 & & & \\
\theta & = & \theta_b & \text{on} \quad \Gamma_b^{in}, \\
\theta & = & \theta_c & \text{on} \quad \Gamma_c^{out}, \\
\dfrac{\partial \theta}{\partial n} & = & 0 & \text{on} \quad \partial\Omega \setminus \{\Gamma_c^{out} \cup \Gamma_b^{in}\}.
\end{array}
\right. \tag{17}
$$

The varying parameters are the velocities $v_b \in [0.5; 2]$, $v_c \in [0.1; 0.4]$ (in mm/s), the imposed temperatures $\theta_b \in [288; 292]$ and $\theta_c \in [295; 315]$ (in Kelvin). For simplicity we will also denoted by $\sigma = (v_b, \theta_b, v_c, \theta_c)$ the set of parameters.

## 4. Numerical results

The blackbox software to compute the pressure, velocity and temperature "truth" and "coarse" approximations is the finite element code "`FreeFem++`"[10]. The $\mathbb{P}_2$-$\mathbb{P}_1$ Taylor-Hood finite element has been used to build the velocity and pressure approximation spaces and the $\mathbb{P}_2$ finite element has been used to build the temperature approximation space over various coarse and fine meshes: $\mathcal{T}_H$ and $\mathcal{T}_h$.

### *4.1. Application 1 : Natural convection in a 2D cavity*

In this example, we consider heat transfer due to natural convection inside a heated cavity as introduced in section 3.2. To start with, we shall focus here on the approximation of the only temperature $\theta$, hence, in the remainder subsection, we have simplified the notation by removing the superscript $\theta$ on $N^\theta$.

In order to build the reduced basis space $X_h^N$, we have computed a "training" sample made of a series of $n_{train} = 93$ fine finite element approximations of (16) for a Prandtl number varying between 0.5 and 1 and a Grashof number varying between $10^3$ and $10^6$ (see Figure 4).

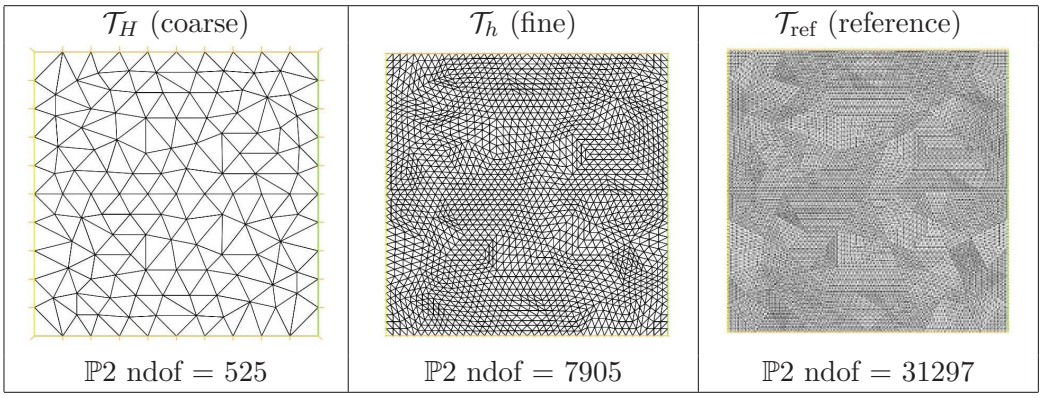


Figure 3: Embedded meshes used to build finite element approximation spaces

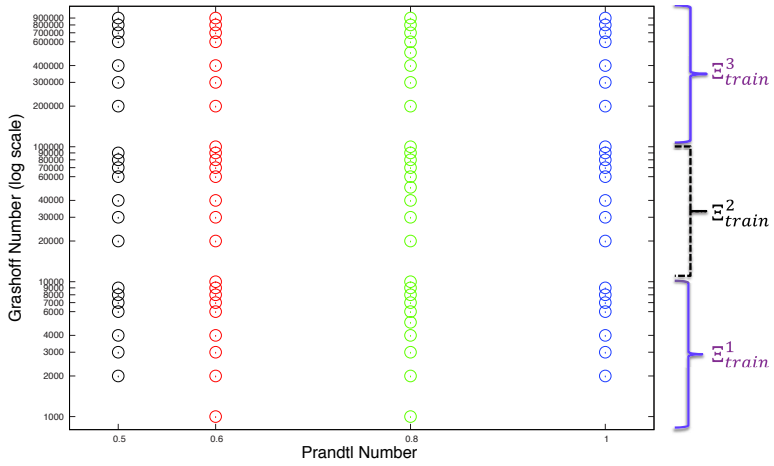


Figure 4: Parameters distribution in $\Xi_{train} = [0.5 : 1] \times [10^3 : 10^6]$

Let us denote by, $\Xi^F_{train}$, the " full training" set of points, in $\mathcal{D}$, associated to our complete "training" sample of finite element approximations. In order to better take into account the disparity between the solutions of lower and higher Rayleigh number ($Ra = Gr \times Pr$), we have decomposed this initial "training" parameter set into three parts (see figure 4) : $\Xi^F_{train} = \Xi^1_{train} \cup \Xi^2_{train} \cup \Xi^3_{train}$ with

$$\begin{cases} \Xi^F_{train} &= [0.5 : 1] \times [10^3 : 10^6], \\ \Xi^1_{train} &= [0.5 : 1] \times [10^3 : 10^4], \\ \Xi^2_{train} &= [0.5 : 1] \times [10^4 : 10^5], \\ \Xi^3_{train} &= [0.5 : 1] \times [10^5 : 10^6]. \end{cases} \tag{18}$$

In order to obtain an optimal set of parameters $\{\sigma_1, \cdots, \sigma_{N_{max}}\}$ from a given training sample $\Xi_{train} \subset \Xi^F_{train}$, we resort to a greedy sampling procedure given in Algorithm 1.

**Algorithm 1** Greedy's algorithm used to choose $\{\sigma_1, \cdots, \sigma_{N_{max}}\}$

Given $\Xi_{train} = (\sigma_1, \cdots, \sigma_{n_t}) \in \mathcal{D}^{n_t}$, $n_t >> 1$ with $n_t \leq n_{train}$ and $\Xi_{train} \subset \Xi^F_{train}$

Choose randomly $\sigma_1$, $\rightarrow S_1 = \{\sigma_1\}$ and $X^1_h = \text{span}\{\theta_h(\sigma_1)\}$

Set $\xi_1 = \dfrac{\theta_h(\sigma_1)}{\|\theta_h(\sigma_1)\|_{L^2}}$

**for** $n = 2$ to $N_{max}$ **do**

$$\sigma_n = \arg \max_{\sigma \in \Xi_{train}} \frac{\|\theta_h(\sigma) - \sum_{i=1}^{n-1} (\theta_h(\sigma), \xi_i)_{L^2}\, \xi_i\|_{L^2}}{\|\theta_h(\sigma)\|_{L^2}}$$

$S_n = S_{n-1} \cup \sigma_n$ and $X^k_h = X^{n-1}_h + \text{span}\{\theta_h(\sigma_n)\}$

Compute $\tilde{\xi}_n = \theta_h(\sigma_n) - \sum_{i=1}^{n-1} \xi_i (\theta_h(\sigma_n), \xi_i)_{L^2}$ and set $\xi_n = \dfrac{\tilde{\xi}_n}{\|\tilde{\xi}_n\|_{L^2}}$

**end for**

Besides, in order to determine the reduced basis's optimal size we propose to look at the behavior of the average error of the rectification process for all the $\sigma \in \Xi_{train} \setminus S_N$ as $N$ increase to $N_{max}$. In order to do so, we computed temporary rectification matrices $\mathbb{T}^N$ associated to the functionals $\{\xi_i\}_{1 \leq i \leq N}$.
To lighten the notation we introduce :
- The vectors $T^i \in \mathbb{R}^N$ for $i = 1, \cdots, N$ defined by

$$(T^i)_j = \mathbb{T}^N_{i,j}, \qquad \forall j = 1, \cdots, N;$$

- The vectors $A^i \in \mathbb{R}^{Nmax}$ for $i = 1, \cdots, N$ defined by

$$(A^i)_k = (\theta_H(\sigma_k), \xi_i)_{L^2} \qquad \forall k = 1, \cdots, N_{max};$$

- The vectors $B^i \in \mathbb{R}^{Nmax}$ defined by

$$(B^i)_k = (\theta_h(\sigma_k), \xi_i)_{L^2}, \qquad \forall k = 1, \cdots, N_{max};$$

- The matrix $D \in \mathbb{R}^{N_{max} \times N}$ defined by

$$D = \begin{pmatrix} A^1 \\ \vdots \\ A^N \end{pmatrix} = \left(\begin{array}{c|c|c} (\theta_H(\sigma_1), \xi_1)_{L^2} & \cdots & (\theta_H(\sigma_1), \xi_N)_{L^2} \\ \vdots & \vdots & \vdots \\ (\theta_H(\sigma_{N_{max}}), \xi_1)_{L^2} & \cdots & (\theta_H(\sigma_{N_{max}}), \xi_N)_{L^2} \end{array}\right).$$

In order to find the optimal coefficients $\mathbb{T}^N_{ij}$ we resort to a least-square recipe with a penalty term. For $1 \leq i \leq N$, we are looking for the vector $T^N_i$ which minimizes the following cost function $C^i$:

$$C^i = \|D\,T^i - B^i\|^2_2 - \lambda \|T^i\|^2_2 \tag{19}$$

where $\lambda$ is a regularization coefficient and $\|\cdot\|_2$ stand for the Euclidian $\ell_2$-norm. We can show that minimization of the cost function(19) leads to a set of $N$ linear equations in the $N$ unknown coefficients $\mathbb{T}^N_{i,j}$ and that it can be written as following the linear system:

$$(D^T D + \lambda\, I_N)\, T^i = D^T B^i \qquad \forall 1 \leq i \leq N,$$

where $I_N$ is the identity matrix in $\mathbb{R}^{N\times N}$. The solution of this equation is :

$$T^i = (D^T D + \lambda\, I_N)^{-1} D^T B^i \qquad \forall 1 \leq i \leq N.$$

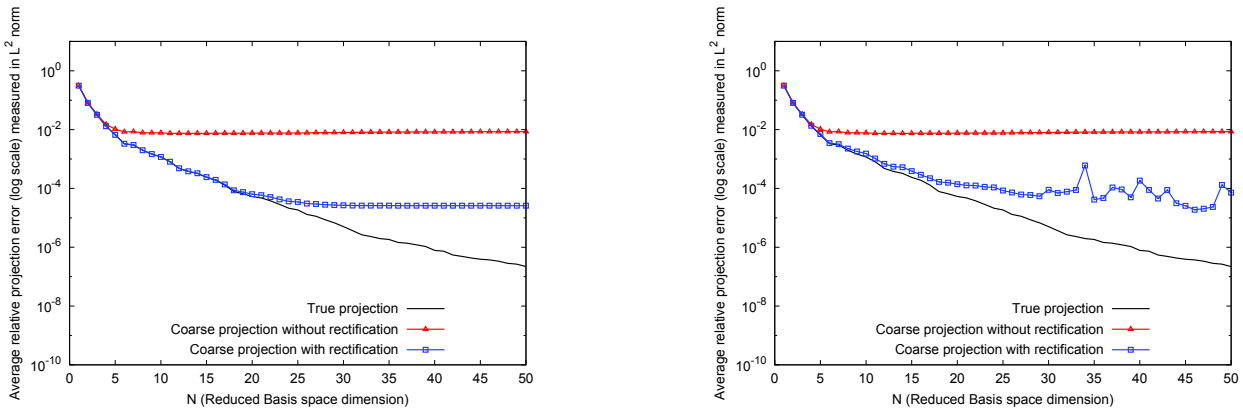


Figure 5: Average errors with $\lambda = 10^{-10}$ (left) and with $\lambda = 0$ (right) during the reduced basis construction stage with $\Xi_{train} = \Xi^F_{train}$

Figure 5 shows for $\Xi_{train} = \Xi^F_{train}$, the behavior of the rectification process with and without the regularization. The average relative errors are measured in $L^2$-norm and defined by :

- for the true projection : $\dfrac{1}{n_{train}} \displaystyle\sum_{k=1}^{n_{train}} \dfrac{\left\| \theta_h(\sigma_k) - \sum_{i=1}^{N} (\theta_h(\sigma_k), \xi_i)_{L^2}\, \xi_i \right\|_{L^2}}{\|\theta_h(\sigma_k)\|_{L^2}}$,

- for the coarse projection without rectification : $\dfrac{1}{n_{train}} \displaystyle\sum_{k=1}^{n_{train}} \dfrac{\left\| \theta_h(\sigma_k) - \sum_{i=1}^{N} (\theta_H(\sigma_k), \xi_i)_{L^2}\, \xi_i \right\|_{L^2}}{\|\theta_h(\sigma_k)\|_{L^2}}$,

- for the coarse projection with rectification : $\dfrac{1}{n_{train}} \displaystyle\sum_{k=1}^{n_{train}} \dfrac{\left\| \theta_h(\sigma_k) - \sum_{i,j=1}^{N} \mathbb{T}^N_{i,j} (\theta_H(\sigma_k), \xi_j)_{L^2}\, \xi_i \right\|_{L^2}}{\|\theta_h(\sigma_k)\|_{L^2}}$.

Without the regularization we observe peaks in the error curve due to a deterioration of the rectified solution when $N$ is large.

Figures 6 and 7 show for the different training sets introduced in (18), the behavior of the rectification process with a regularization term $\lambda$ set to $10^{-10}$ in order to insure a robust process.

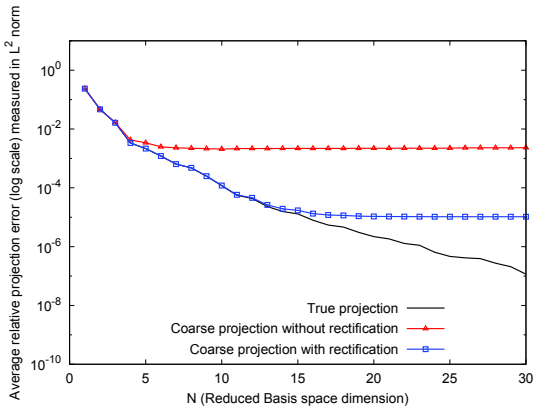


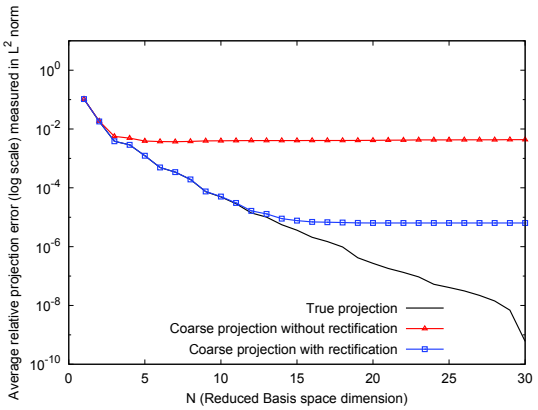


Figure 6: Average errors during the reduced basis construction stage with $\Xi_{train} = \Xi^1_{train} \cup \Xi^2_{train}$ (left) and with $\Xi_{train} = \Xi^2_{train}$ (right)

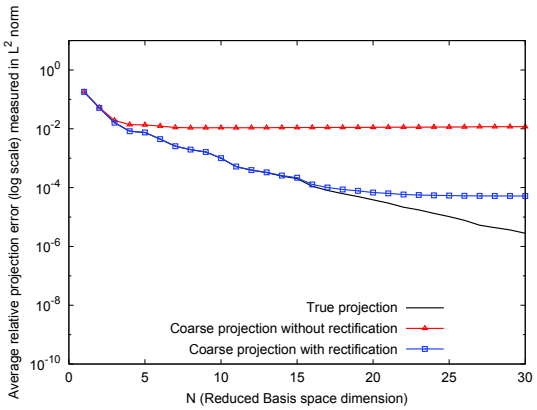


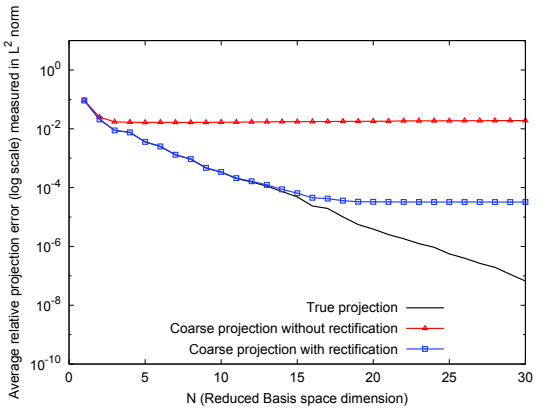


Figure 7: Average errors during the reduced basis construction stage with $\Xi_{train} = \Xi^F_{train} \setminus \Xi^1_{train}$ (left) and $\Xi_{train} = \Xi^3_{train}$ (right)

With the regularization, the rectification process remains good when $N$ is large, despite the fact that a threshold in the error is reached. Reminding that, as proven in [3, 4, 15], we have

$$\|\theta(\sigma) - R_N\theta_H(\sigma)\|_{H^1} \leq c_1(N)(h + H^2) + \varepsilon(N),$$

where $R_N\ \theta_H(\sigma) = \sum_{i,j=1}^{N} \mathbb{T}^N_{i,j}\,(\theta_H(\sigma), \xi_j)_{L^2}\,\xi_i$. The behavior of the rectified solution $R_N\theta_H(\sigma)$ observed when $N$ is large in figures 6 and 7 confirms that constant $c_1(N)$ is growing with $N$.

Finally, we have decided to stop the enrichment of the reduced basis space when the rectification error stop decreasing rapidly and reach a threshold (see table 2).

| Parameter space $\Xi_{train}$ | $N_{max}$ |
|---|---|
| $\Xi^F_{train}$ | 30 |
| $\Xi^1_{train} \cup \Xi^2_{train}$ | 20 |
| $\Xi^2_{train}$ | 15 |
| $\Xi^F_{train} \setminus \Xi^1_{train}$ | 20 |
| $\Xi^3_{train}$ | 20 |

Table 2: Value of $N^{\theta}_{max}$ for a variety of $\Xi_{train}$

Figure 8, below shows the parameters distribution during the reduced basis construction stage with $\Xi_{train} = \Xi^F_{train}$.

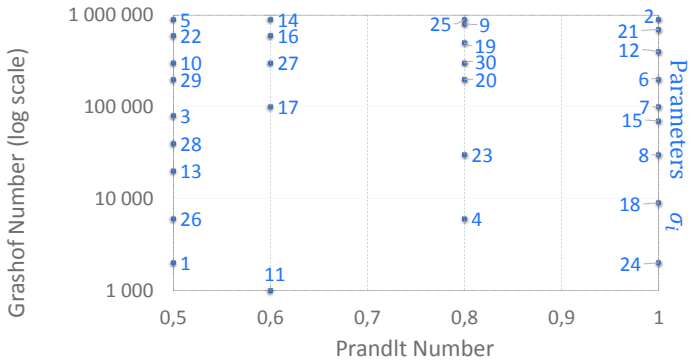


Figure 8: Parameters distribution during the reduced basis construction stage with $\Xi_{train} = \Xi^F_{train}$

Once we have determined, for each parameter space $\Xi_{train}$, the set of parameters $\{\sigma_1, \cdots, \sigma_{N_{max}}\}$ that will be used to generate $X^h_N$, we solve, for several values of $N \leq N_{max}$, the following eigenvalue problem: find $(\lambda_k, \Phi_k) \in \mathbb{R}^N \times \mathbb{R}^N$, $1 \leq k \leq N$ such that

$$\mathrm{K}^N \, \Phi_k = \lambda_k \, \mathrm{M}^N \, \Phi_k \qquad \text{with } \mathrm{M}^N_{i,j} = \int_\Omega \xi_i \, \xi_j \text{ and } \mathrm{K}^N_{i,j} = \int_\Omega \nabla \xi_i \, \nabla \xi_j.$$

Which will provide $N$ basis functions of $X^N_h$ orthogonalized in $L^2$ and $H^1$ norm, defined as

$$\phi^{\theta,N}_k = \frac{1}{\sqrt{\lambda_k}} \sum_{i=1}^{N} (\Phi_k)_i \, \xi_i.$$

To validate the reduced basis functions, we have looked at the convergence rate of the $H^1$-orthogonal projection from $X_h$ into $X^N_h$ for some particular solutions $\theta_h(\sigma)$, with $\sigma \in \mathcal{D} \setminus \Xi_{train}$ depending on the parameters space $\Xi_{train}$. Figure 9 shows the temperature field $\theta_h(\sigma)$ with a lower Rayleigh number (on the left side) and a higher Rayleigh number (on the right side).

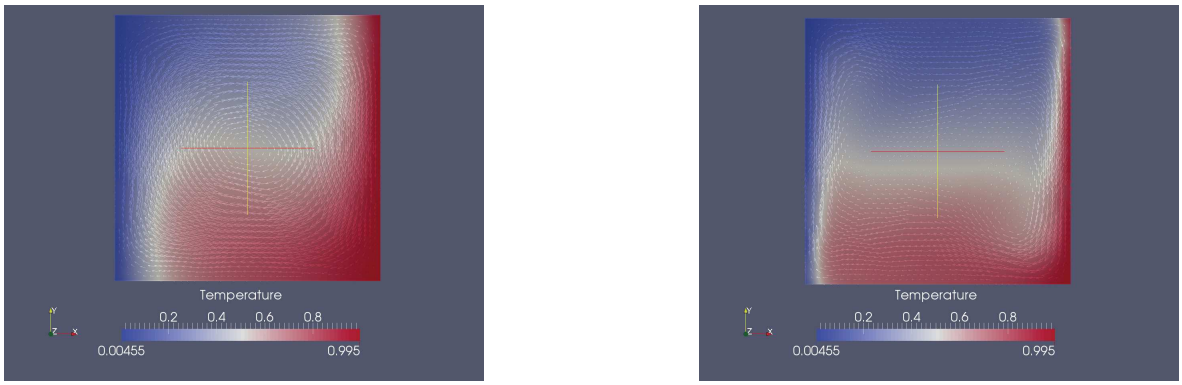


Figure 9: Temperature field $\theta_h(\sigma)$ (on the left with $\sigma = (0.75; 25\,000)$ and on the right with $\sigma = (0.7; 750\,000)$)

Let the projection error measured in $H^1$-norm defined by

$$\|\Pi_N \theta_h(\sigma) - \theta_{ref}(\sigma)\|_{H^1} = \frac{\left\| \sum_{i=1}^{N} (\theta_h(\sigma_k), \phi_i^{\theta,N})_{H^1} \, \phi_i^{\theta,N} - \theta_{ref}(\sigma) \right\|_{H^1}}{\|\theta_{ref}(\sigma)\|_{H^1}},$$

where $\theta_{ref}(\sigma)$ is a reference FEM solution computed on the reference mesh $\mathcal{T}_{ref}$ (see figure 3). Figure 10 shows that the projection error is same as the fine FEM error for $N = N_{max}$.

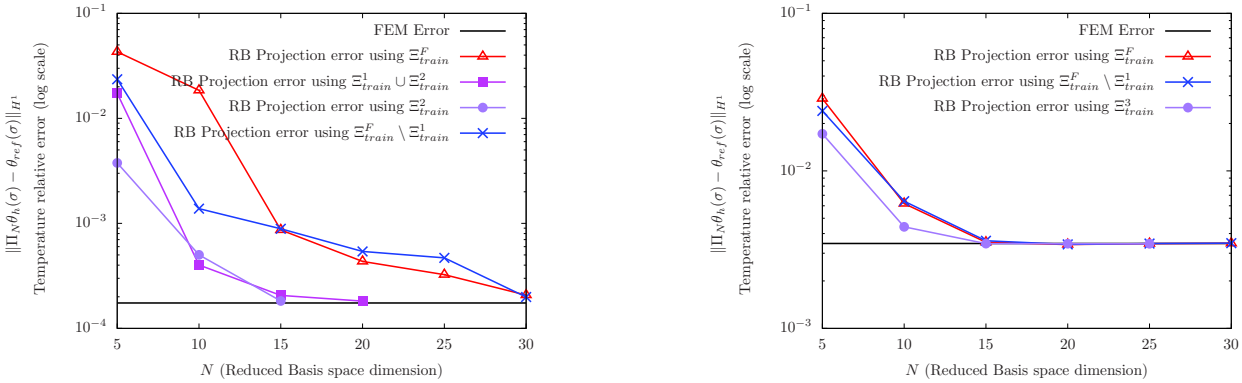


Figure 10: Convergence rate of the reduced basis's projection measured in $H^1$-norm (on the left with $\sigma = (0.75; 25\,000)$ and on the right with $\sigma = (0.7; 750\,000)$)

In the figure 11 we can see the convergence rate of the non-intrusive reduced basis (NIRB) approximation $\theta^N_{H,h}$ as function of $N$ for some particular value of $\sigma \in \mathcal{D} \setminus \Xi_{train}$ depending on the parameters space $\Xi_{train}$. We defined the relative NIRB error measured in $H^1$-norm by

$$\frac{\left\| \sum_{i,j=1}^{N} R^{\theta,N}_{i,j} (\theta_h(\sigma_k), \phi_j^{\theta,N})_{L^2} \, \phi_i^{\theta,N} - \theta_{ref}(\sigma) \right\|_{H^1}}{\|\theta_{ref}(\sigma)\|_{H^1}},$$

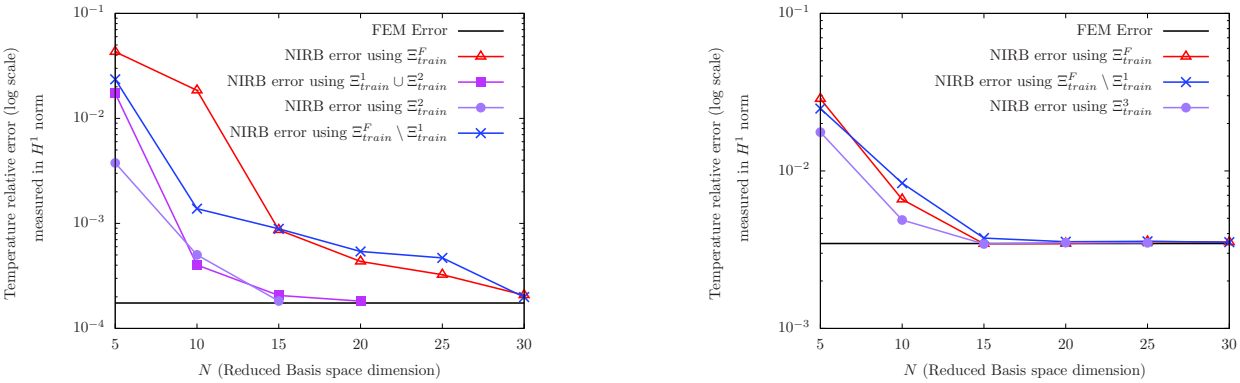


Figure 11: Convergence rate of the improved reduced basis approximation $\theta^N_{H,h}$ as function of $N$ measured in $H^1$-norm during the online stage (on the left with $\sigma = (0.75; 25\,000)$ and on the right with $\sigma = (0.7; 750\,000)$)

As we expected, we were able to reach the same accuracy as the fine finite element solution and to reduced significantly the computational times (see table 3).

| F.E.M. Fine sol. | NIRB method (on line stage) | | | |
|---|---|---|---|---|
| | FEM coarse sol. | Rectification | | |
| | | N=15 | N=20 | N=30 |
| 7min28 | 26 sec | 5 sec | 9 sec | 19 sec |

Table 3: Average execution's times

### *4.2. Application 2 : Cooling system of electronic devices*

In this second example, we are interested in the evaluation of the velocity and the temperature inside a simplified cooling system for electronics devices.

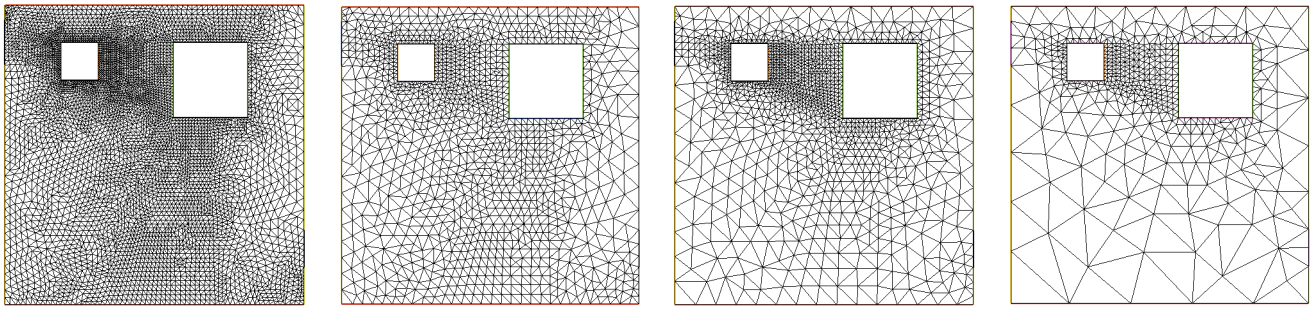

$\mathcal{T}_h$ $\mathbb{P}2$ Ndof = 20213 | $\mathcal{T}_{H_1}$ $\mathbb{P}2$ Ndof = 5148 | $\mathcal{T}_{H_2}$ $\mathbb{P}2$ Ndof = 5088 | $\mathcal{T}_{H_3}$ $\mathbb{P}2$ Ndof = 1871

Figure 12: From the left to the right : fine mesh ($\mathcal{T}_h$), embedded coarse mesh ($\mathcal{T}_{H_1}$), non embedded coarse mesh ($\mathcal{T}_{H_2}$), non embedded very coarse mesh ($\mathcal{T}_{H_3}$).

In order to build the reduced spaces $X^N_h$ and $Y^N_h$ we have used a fine finite element mesh with 20,213 degrees of freedom (mesh $\mathcal{T}_h$ in Figure 12). In order to test the NIRB on various coarse meshes, we have

computed a sample of coarse and fine finite element approximations of problem (17), using embedded or non embedded meshes (see figure 12). The associated parameters space — denoted by $\Xi^{train}$ — is of size 120, and composed of parameters within the following values:

| $\theta_b$ | $v_b$ | $v_c$ | $\theta_c$ |
|---|---|---|---|
| 288 | 0.5 | 0.1 | 295 |
| 292 | 1 | 0.2 | 300 |
| | 2 | 0.3 | 305 |
| | | 0.4 | 310 |
| | | | 315 |

To verify the non-intrusive reduced basis method, we have compared the fine finite element solution for $\sigma = (\theta_b; v_b; v_c; \theta_c) = (290; 1.5; 0.25; 312)$ (see figure 13) with different reduced solutions (see Figure 14).

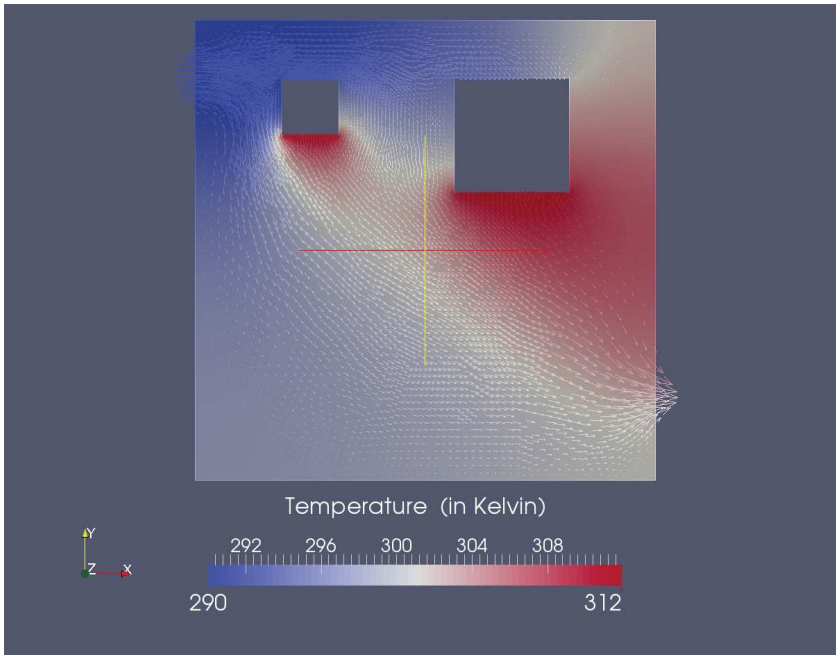


Figure 13: Temperature field for $\sigma = (\theta_b; v_b; v_c; \theta_c) = (290; 1.5; 0.25; 312)$

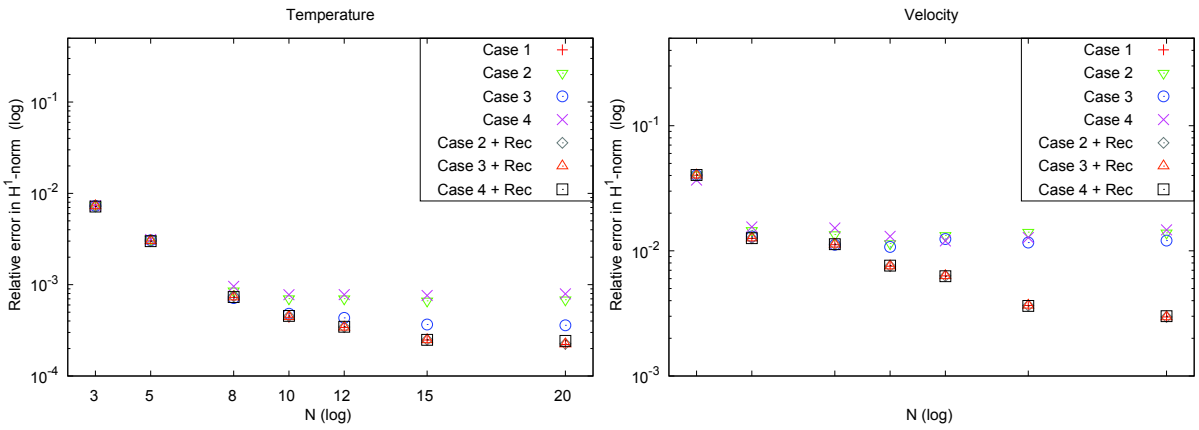


Figure 14: Relative error between the fine FEM solution and the various reduced solutions measured in $H^1$-norm (temperature on the left and velocity on the right).

- **Case 1**:
  In this example, we want to see the error due only to the reduced basis size $N$. To do so, as in the previous section, we have computed the $L^2$ projection of the fine finite element solution on the reduced basis space.

  For a given $N$, those solutions are the best approximation that we can expect in the reduced basis space.

- **Case 2, 3 and 4**:
  In those examples, we wanted to see how the choice of the coarse mesh $\mathcal{T}_H$ affect the NIRB method when there is no rectification.
  We have used embedded coarse mesh ($\mathcal{T}_H = \mathcal{T}_{H_1}$) and not embedded coarse meshes ($\mathcal{T}_H = \mathcal{T}_{H_2}$ or $\mathcal{T}_{H_3}$) to compute the reduced approximation in respectively the case 2, 3 and 4.
  We notice that as N goes larger the error between the different reduced solutions and the FEM solution goes smaller to finally reach a threshold. This is due to the fact that the coarse finite element's error become more significant than the reduced basis size's error.

**Remark** *: From a practical viewpoint, we want to use a finite element software able to compute the coefficients $\gamma_j^{H_i}(\sigma)$ easily and in a way that it is not too time consuming. Indeed, in order to do compute those coefficients we resort to numerical integration. However, in the case when the meshes are not embedded a supplementary difficulty arise from the fact that the reduced basis functions and the coarse solutions do not belong to a same finite element space. We want to avoid an extra interpolation error due to the interpolation of the coarse solution to the reference mesh. It is made by the use of a numerical quadrature formula over each triangle $K_h$ based Gauss points, here we choose a $\mathbb{P}_2$-unisolvent formula (with 7 points). For example $\int_{K_h} \theta_{H_i}(\sigma)\xi_h^j$ will be replaced by $\sum_{p=1}^{7} \omega_p \times \theta_{H_i}(x_p;\sigma) \times \xi_h^j(x_p)$, where $\omega_p$ are the weight of the quadrature point. Then to compute $\theta_{H_i}(x_p;\sigma)$, we just have to find in which triangle of $\mathcal{T}_{H_i}$ belongs the point $x_p$, to avoid any interpolation of $\theta_{H_i}(\sigma)$ on $K_h$. In the software that we have used for our numerical experiments, this step was done automatically.*

- **Case 2 + Rec, 3 + Rec and 4 + Rec** : In those examples we wanted to see the influence of the rectification on the reduced solution. We observe that with this rectification we are able to reach the same accuracy as if we have projected the reference finite element solution on the reduced basis space, even with the coarsest mesh. In particular, when using coarse mesh $\mathcal{T}_{H_3}$, we are able to divide the computational times by 10 without any loss of accuracy (see figures 15 and 16).

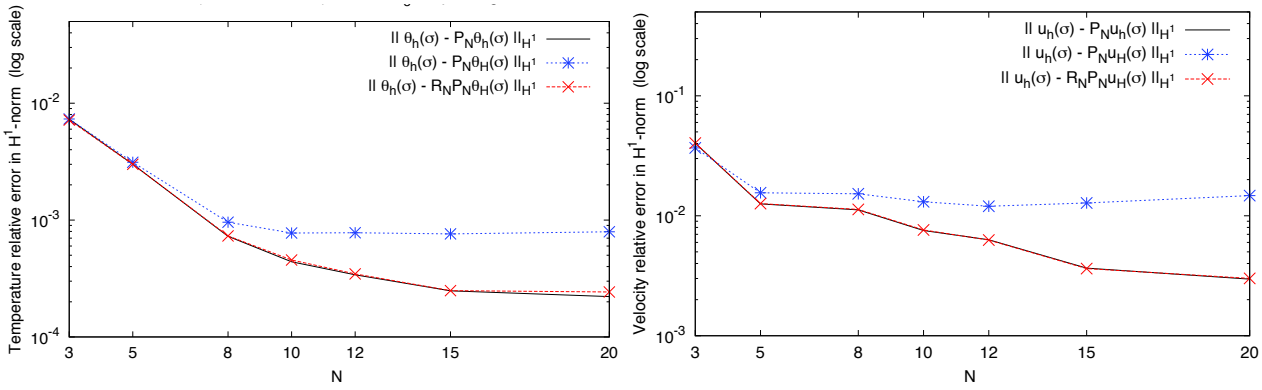


Figure 15: Relative error between the fine FEM solution the various reduced solutions measured in $H^1$-norm with $T_H = T_{H_3}$ (temperature on the left and velocity on the right).

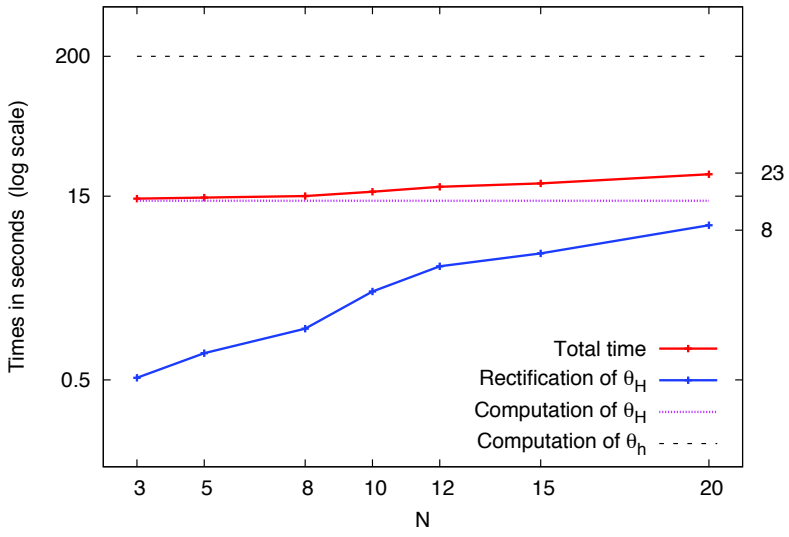


Figure 16: Comparison of CPU Times between the fine FEM and the NIRB method

### *4.3. Conclusion*

The present paper illustrates the capability of non-intrusive reduced basis method to return computationally efficient and accurate thermal flux for simple model of cooling systems. Coarse triangulations have been used to compute finite element solutions during the online stage. In order to regain accuracy,

we first project these solutions into the RB space, and then improve them via a rectification technique. Our numerical results prove that the two ingredients i) projection ii) rectification, are inseparable in order to get the expected accuracy. With this approach, we are still able to significantly reduce our computational cost without modifying the CFD code, and it is thus user-friendly. The only thing that we need to get out the plain CFD finite element software are: i) the meshes (fine and coarse) and ii) the nodal values of each fields we want to approximate, in order to export these data in a simple finite element code (as e.g. Matlab, FEEL++, FreeFem++) where simple $L^2$ and $H^1$ scalar products are performed. Our simulations also illustrate that the coarse and fine meshes do not need to be embedded.

**Acknowledgment**

The authors would like to graciously thank Pascal Joly for fruitful discussions and very valuable advice in the beginning of our project. This work was partially supported by the Research Grant FNRAE RB4FASTSIM.

## 5. References

[1] A. Buffa, Y. Maday, A.T Patera, C. Prud'homme and G. Turinici *A priori convergence of the Greedy algorithm for the parametrized reduced basis method* ESAIM: M2AN, 46 3 (2012) 595-603

[2] T. Chacón Rebollo, E. Delgado Ávila, M. Gómez Mármol, F. Ballarin, and G. Rozza, *On a certified Smagorinsky reduced basis turbulence model*, SIAM Journal on Numerical Analysis (2017).

[3] R. Chakir and Y. Maday. *Une méthode combinée d'éléments finis à deux grilles/bases réduites pour l'approximation des solutions d'une E.D.P. paramétrique.* C. R. Acad. Sci. Paris, Ser. I Vol 347, p435-440 (2009).

[4] R. Chakir and Y. Maday. *A two-grid finite-element/reduced basis scheme for the approximation of the solution of parameter dependent P.D.E.* Actes de congrès du 9ème colloque national en calcul des structures, Giens 2009.

[5] W.Chen, J. Hesthaven, B. Junqiang, Z. Yang and Y. Tihao, *A greedy non-intrusive reduced order model for fluid dynamics* American Institute of Aeronautics and Astronautics (2017)

[6] N.N. Cuong, N. Veroy and A.T. Patera, *Certified real-time solution of parametrized partial differential equations*. Handbook of Materials Modeling, 1529-1564, (2005).

[7] S. Deparis. *Reduced basis error bound computation fo parameter - dependant Navier-Stokes equations by natural norm approach.* SIAM J. Numer. Anal. Vol 46, p 2039-2067 (2008).

[8] S. Deparis and G. Rozza. *Reduced basis method for multi-parameter-dependent steady Navier-Stokes equations: Applications to natural convection in a cavity.* Journal of Computational Physics, Vol 228, No 12, p4359-4378 (2009).

[9] M. Grepl, Y. Maday, N. Nguyen, and A.T Patera. *Efficient reduced-basis treatment of nonaffine and nonlinear partial differential equations*, M2AN, Vol 41, No 3, p575-605 (2007).

[10] F. Hecht *New development in FreeFem++.* Journal of Numerical Mathematics, 20(3-4), pp. 251-266 (2012)

[11] J. Hesthaven, B. Stamm, S. Zhang,*Efficient greedy algorithms for high-dimensional parameter spaces with applications to empirical interpolation and reduced basis methods*, ESAIM-Math. Model. Num., Vol. 48, pp. 259-283 (2014)

[12] K. Ito and S.S. Ravindran. *A reduced-order method for simulation and control of fluid flow.* J. Computat. Phys., Vol 143, p403-425 (1998).

[13] A. Lovgren, Y. Maday and E. Ronquist . *A reduced basis element method for the steady Stokes problem.* ESAIM: Mathematical Modelling and Numerical Analysis, 40, pp 529-552, (2006).

[14] Y. Maday. *Reduced basis method for the rapid and reliable solution of partial differential equations.* in International Congress of Mathematicians, Vol. III, p1255-1270, Eur. Math. Soc. Zurich (2006).

[15] O. Mula *Quelques contributions vers la simulation parallèle de la cinétique neutronique et la prise en compte de données observées en temps réel.* Phd thesis, Université Pierre et Marie Curie (2014).

[16] J.S. Peterson. *The reduced basis method for incompressible viscous flow calculations.* SIAM Journal on Scientific and Statistical Computing, Vol 10, No 4 p777-786 (1989).

[17] C. Prud'homme, D. Rovas, K. Veroy, L. Machiels, Y. Maday, A. Patera, and G. Turinici. *Reliable real-time solution of parametrized partial differential equations: Reduced-basis output bound methods.* J Fluids Engineering, Vol 124 p70-80 (2002).

[18] A. Quarteroni and G. Rozza. *Numerical Solution of Parametrized Navier-Stokes Equations by Reduced Basis Methods* Numer. Methods Partial Differential Equations, Vol 23, No 4, p923-948 (2007).

[19] A. Quarteroni, G. Rozza, and A. Manzoni. *Certified Reduced Basis Approximation for Parametrized Partial Differential Equations and Applications.* Journal of Mathematics in Industry 2011 Vol 1, No 3 (2011).

[20] G. Rozza. *Reduced Basis Approximation and Error Bounds for Potential Flows in Parametrized Geometries* Commun. Comput. Phys. Vol 9, No 1, p1-48 (2011).

[21] G. Rozza, D.B.P Huynh, N.C. Nguyn and A.T. Patera *Real-time reliable simulation of heat transfer phenomena*, Proceeding of HT2009, ASME Summer Heat Transfer Conference (2009).

[22] G. Rozza and K. Veroy, *On the stability of the reduced basis method for Stokes equations in parametrized domains*, Computer Methods in Applied Mechanics and Engineering, Volume 196, Issue 7, 10, p1244-1260 (2007).

[23] G Pitton, A Quaini and G Rozza, *Computational reduction strategies for the detection of steady bifurcations in incompressible fluid-dynamics: Applications to Coanda effect in cardiology* Journal of Computational Physics, Volume 344, p534-557, (2017)

[24] E. Schenone, S. Veys and C. Prud'homme, *High Performance Computing for the Reduced Basis Method. Application to Natural Convection.* ESAIM: Proceedings, 43, p255-273. (2013).

[25] O. Souhar and C. Prud'homme, *Numerical analysis method of heat transfer in an electronic component using sensitivity analysis.* Journal of Computational Electronics. 13 (4), p1042-1053 (2014).

[26] L. Fick, Y. Maday, A.T Patera and T. Taddei *A Reduced Basis Technique for Long-Time Unsteady Turbulent Flows*, arXiv:1710.03569

[27] K. Veroy and A.T. Patera. *Certified real-time solutions of the parametrized steady incompressible Navier-Stokes equations.* International Journal for Numerical Methods in Fluids, Vol 47, p773-788 (2005).

[28] D. Xiao, F. Fang, A.G. Buchan, C.C. Pain, I.M. Navon, J. Du, G. Hu, , *Non-linear model reduction for the Navier-Stokes equations using residual DEIM method*, Journal of Computational Physics, Vol 263, p1-18 (2014).

[29] D. Xiao, F. Fang, C.C. Pain and I.M. Navon, *A parameterized non-intrusive reduced order model and error analysis for general time-dependent nonlinear partial differential equations and its applications* Computer Methods in Applied Mechanics and Engineering Vol 317, p868-889 (2017)